Journal of Hydrology 519 (2014) 238–247

Contents lists available at ScienceDirect

Journal of Hydrology

journal homepage: www.elsevier.com/locate/jhydrol

Axisymmetric gravity currents within porous media: First order solution and experimental validation

Sandro Longo [a,*], Vittorio Di Federico [b]

[a] Dipartimento di Ingegneria Civile, Ambiente Territorio e Architettura (DICATeA), Università di Parma, Italy
[b] Dipartimento di Ingegneria Civile, Chimica, Ambientale e dei Materiali (DICAM), Università di Bologna, Italy

ARTICLE INFO

Article history:
Received 17 January 2014
Received in revised form 15 June 2014
Accepted 2 July 2014
Available online 10 July 2014
This manuscript was handled by Peter K. Kitanidis, Editor-in-Chief, with the assistance of Todd C. Rasmussen, Associate Editor

Keywords:
Gravity current
Porous
Similarity solution
Rayleigh expansion
Experimental results

SUMMARY

Spreading of gravity currents in porous media has traditionally been investigated analytically by means of similarity solutions under the Dupuit–Forchheimer approach. We present a novel formulation to analyse the axisymmetric propagation of single-phase gravity currents induced by the release of a time-variable volume of fluid in a porous domain. Our approach is based on a first order expansion of the velocity potential that allows for the presence of vertical Darcy velocities. Coupling the flow law with mass balance equations leads to a PDE which admits a self-similar solution for the special case in which the volume of the fluid fed to the current increases at a rate proportional to t^3. A numerical solution is developed for rate proportional to t^α with $\alpha \neq 3$. Current profiles obtained with the first order solution have a finite height at the origin. Theoretical results are compared with two experimental datasets, one having freshwater and the other air as an ambient fluid. In general, experimental current profiles collapse well onto the numerical results; the first order solution shows a marked improvement over the zeroth order solution in interpreting the current behaviour near the injection point. A sensitivity and uncertainty analysis is conducted on both the first order and zeroth order theoretical model. The sensitivity analysis indicates that the flow process is more sensitive to porosity variations than to other parameters. The uncertainty analysis of the present experimental data indicates that the diameter of glass beads in an artificial porous medium is the source of most of the overall uncertainty in the current profile.

1. Introduction

Flows in porous media driven by the force of gravity acting on density differences between an intruding and an ambient fluid are usually termed gravity currents, and are frequent in many environmental and industrial processes. Notable examples include injection of gas or liquid into natural reservoirs to improve recovery of oil and heat, release of agents or environmental carriers into aquifers for remediation of groundwater contamination, carbon dioxide sequestration in deep formations to reduce greenhouse gas emissions, and saltwater intrusion in coastal aquifers. These important applications, with far-reaching economic implications, have prompted in the past three decades the development of significant research advances, both of theoretical and experimental nature, on the propagation of gravity currents in porous media. Among these, a number of closed-form approaches were developed to analyse one-phase flows in a variety of geometric settings and with different boundary conditions. Noteworthy examples include flow over an horizontal surface in plane (Huppert and Woods, 1995) and radial geometry (Lyle et al., 2005) generated by an instantaneous or continuous release of fluid. These solutions were extended to incorporate two-layer flow (Woods and Mason, 2000), the effect of a sloping bottom (Vella and Huppert, 2006; Koussis et al., 2012), the action of impermeable confining boundaries (Golding and Huppert, 2010), and drainage effects (Pritchard et al., 2001). In other cases, the volume of fluid injected in the origin of a semi-infinite porous domain is not conserved, as the fluid mound partially drains back; the corresponding initial value problem for an instantaneous injection is known as the dipole, as the first spatial moment of the mound is conserved. The closed-form solution to this problem, originally derived by Barenblatt and Zel'dovich (1957), was extended by King and Woods (2003) to include drainage and by Mathunjwa and Hogg (2007) to incorporate a vertical variation in permeability.

All of these studies rely on a thin-current assumption, in which the component of Darcy flow perpendicular to the main direction

* Corresponding author.
E-mail addresses: sandro.longo@unipr.it (S. Longo), vittorio.difederico@unibo.it (V. Di Federico).

http://dx.doi.org/10.1016/j.jhydrol.2014.07.003
0022-1694/

of motion is neglected, applying the Dupuit–Forchheimer approximation. This entails a logarithmic singularity at the origin of a radial coordinate system, as clearly shown by Dussan and Auzerais (1993) and further discussed by Li et al. (2005) and Di Federico et al. (2012).

Several different approaches were developed to remove this approximation and describe the flow field more accurately. Dagan (1967) derived a second order approximate theory for steady free surface 2-D flow in porous media via matched asymptotic expansions, demonstrating that the zero order term of the expansion coincides with the Dupuit–Forchheimer approximation. He adopted a general shallow-flow expansion introducing a small parameter to stretch differently the horizontal and the vertical coordinates, then assumed an expansion of the potential involving powers of the square of the small parameter; the series included only even powers to match the inner and the outer expansion. An extension to axisymmetric geometry to deal with pumping wells was developed with a similar mathematical technique by Dagan (1968). The modelling of groundwater periodic motion in aquifers, as generated by tidal excursions, often requires an extension of the zeroth order theory in order to include the effects of vertical velocity and remove the hydrostatic hypothesis. To this purpose, a shallow water expansion was adopted in Parlange et al. (1984) to evaluate a hierarchy of functions representing the terms of a series development of the hydraulic head.

An asymptotic expansion in the vertical-to-horizontal aspect ratio was adopted by Yortsos (1995), who also included the effects of different permeabilities in the vertical and horizontal direction. He demonstrated rigorously that the Dupuit approximation (and several other approximations in different contexts) is obtained considering only the leading order term of the expansion.

A step-wise approach, where the zeroth order term corresponds to the Dupuit–Forchheimer approximation, was adopted in Nielsen et al. (1997) to model tidal water table waves. They introduced the effects of a vertical velocity varying linearly in the vertical on the pressure field. A similar approach is also reported in Knight (2005) for several test-case problems.

In a similar way, Nordbotten and Celia (2006) developed a scheme to correct the vertical equilibrium model (i.e., Dupuit approximation) by introducing a vertical velocity with a linear variation, that was observed in numerous numerical simulation; as a consequence, the pressure variation in the vertical is quadratic. de Loubens and Ramakrishnan (2011) gave a formal justification of the vertical equilibrium approach through a perturbation theory, without making assumptions on the pressure distribution.

Here, we adopt a series expansion of the velocity potential which is polynomial in the vertical coordinate and contains only even terms as a consequence of the no-flow boundary condition at the horizontal bottom. The asymptotic expansion is in power of a small parameter equal to the ratio between vertical and horizontal length scales; at the zeroth order, it reduces to the Dupuit approximation, like the approaches of other researchers. All the terms in the series are expressed iteratively as space derivatives of the zeroth order potential. While other approaches (e.g., Dagan, 1967) adopt a series with only even powers, to our knowledge the derivation of the higher order terms as a function of the zeroth order term is novel in the field of flow in porous media. This relationship is an advantage since it allows the direct implementation of the effects at every order without a hierarchical approach, albeit with an increase in the order of the differential problem describing the physical processes.

The aforementioned approach is used to derive a first order correction to the similarity solution developed by Lyle et al. (2005) to analyse the spreading of a gravity current in a porous medium in radial geometry. The solution thereof was successfully used to interpret accumulation of supercritical carbon dioxide beneath low-permeability mudstone layers at the Sleipner site in the North Sea (Bickle et al., 2007), following injection of CO_2 at an approximately constant rate since 1996. An extension of their formulation allowing for nonzero vertical components of the velocity field may be of interest also in view of recent further refinements of the model incorporating two-phase flow (Golding et al., 2013). The present approach can be of interest also in all flows characterised by relevant gradient of the interface and possibly in non stationary conditions, such as coastal salt water intrusion under the effect of tidal fluctuations.

The paper is organised as follows. Section 2 presents the theoretical formulation of the problem, while Section 3 illustrates the results, obtained with self-similar transformation in the special case $\alpha = 3$ and via numerical integration in the general case. In Sections 4 and 5, theoretical results are compared with laboratory experiments. Section 4 describes the experimental apparatus used by Longo et al. (2013) to analyse the spreading of gravity currents in porous media, and illustrates the comparison with their experiments. Throughout the analysis, the sources of uncertainty in the modelling approach and their respective weights are highlighted. A systematic comparison with results from a second experimental dataset by Lyle et al. (2005) is presented in Section 5 following the same approach. A more extensive comparison of the theoretical model with experimental results is available online as Supplementary Material.

A set of conclusions (Section 6) closes the paper, while the Appendix includes further details on the model sensitivity analysis.

2. Formulation of the problem

Consider an axisymmetric gravity current of a Newtonian liquid of density ρ propagating above an horizontal impermeable boundary and intruding in an infinite porous domain of depth h_0, saturated with an ambient fluid of density $\rho - \Delta\rho$ (Fig. 1).

The current is released into the porous medium by a line source along the vertical axis, extends from the origin to a coordinate denoted by $r_N(t)$, and has a volume given by Qt^α, where Q and α are positive constants, and $\alpha = 0$ and $\alpha = 1$ indicate respectively an instantaneous release of a fixed volume and a constant volume influx; the actual discharge for $\alpha \neq 0$ is given by $Q_d = \alpha Q t^{\alpha-1}$. The equation of mass conservation is

$$\nabla \cdot \mathbf{u} = 0, \tag{1}$$

with $\mathbf{u} = (u, w)$ representing Darcy velocity, given by Darcy's law (Bear, 1988; Phillips, 1991; Dullien, 1992):

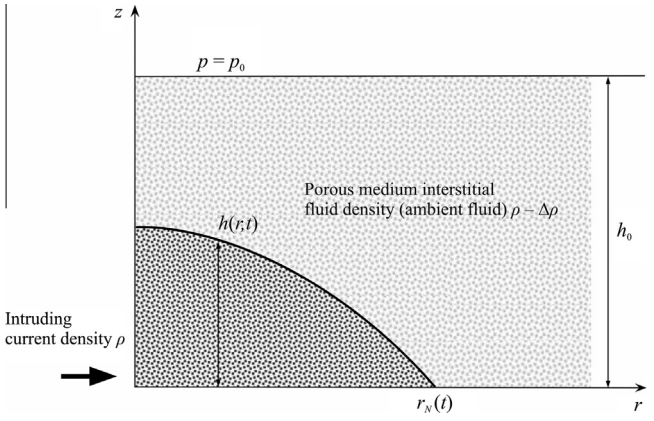

Fig. 1. Layout of the problem.

$$\mathbf{u} = -\frac{k(\phi)}{\mu}(\nabla p + \rho g \mathbf{j}), \tag{2}$$

where $\mathbf{j}$ is a unit vector in the vertical direction, p the pressure, μ the dynamic viscosity, k and ϕ the porous medium intrinsic permeability and porosity, respectively. We assume that the intruding current is relatively thin when compared to the thickness h_0 of the porous domain, allowing to neglect the dynamics of the ambient fluid. This assumption may become questionable at the later stages of a continuous injection, if the volume increase of the current is rapid enough to determine an increase of the height of the current with time at a given location. Hence adhering to this hypothesis places limitations on the value of the injection parameter α and other problem parameters; for a discussion see Golding and Huppert (2010) and Di Federico et al. (2014). We further assume the validity of the sharp interface approximation, allowing to describe the intrusion essentially via a single height function. The resulting model is valid until diffusion and dispersion effects influence considerably the dynamics of the current. The interface is considered to be stable, and surface tension effects are taken to be negligible, as there is no capillary entry pressure limiting the migration of the injected fluid through the pores of the medium. Under these hypotheses, the boundary between the current and the ambient fluid is described by the equation $F(r,z,t) \equiv z - h(r,t) = 0$, with $h(r,t) \ll h_0$ being the current height. The kinematic condition at the interface requires that

$$\frac{\partial h}{\partial t} + u\frac{\partial h}{\partial r} = w, \text{ at } z = h, \tag{3}$$

while the boundary condition at the leading edge is

$$h = 0, \text{ at } r = r_N(t). \tag{4}$$

The additional boundary conditions are

$$\begin{aligned} &w = 0, \text{at } z = 0, \\ &p = p_0 + (\rho - \Delta\rho)g(h_0 - h), \text{at } z = h. \end{aligned} \tag{5a,b}$$

Implying respectively an impervious horizontal bottom and an hydrostatic pressure distribution in the ambient fluid, where p_0 is the pressure at the level h_0. Conditions (5a,b) and (4) inserted in Eq. (3) state that the front end of the intruding current moves with the horizontal fluid velocity at the contact line

$$\frac{dr_N}{dt} = u_N. \tag{6}$$

Combining the mass balance Eq. (1), the kinematic conditions at the interface (3) and at the bottom (5a), and the hydrostatic assumption in the ambient fluid (5b) results in (e.g. Ungarish, 2010)

$$\frac{1}{r}\frac{\partial}{\partial r}(r\bar{u}h) = -\phi\frac{\partial h}{\partial t}, \tag{7}$$

where $\bar{u}$ is the z-averaged radial velocity of the current.

By introducing the potential field variable $\varphi = p/\rho g + z$, Eqs. (1) and (2) are recast for a homogeneous flow field as

$$\nabla^2\varphi = 0 \tag{8}$$

with the boundary conditions

$$\begin{aligned} &\frac{\partial\varphi}{\partial z} = 0, \quad \text{at } z = 0, \\ &\varphi = \frac{\rho - \Delta\rho}{\rho}h_0 + \frac{p_0}{\rho g} + \frac{\Delta\rho}{\rho}h, \quad \text{at } z = h, \end{aligned} \tag{9a,b}$$

where $(\rho - \Delta\rho)h_0/\rho + p_0/\rho g$ can be set to zero without loss of generality.

In axisymmetric geometry, the components of Darcy velocity are given by

$$\begin{aligned} u &= -\frac{k\rho g}{\mu}\frac{\partial\varphi}{\partial r}, \\ w &= -\frac{k\rho g}{\mu}\frac{\partial\varphi}{\partial z}, \end{aligned} \tag{10a,b}$$

where the tangential velocity has been neglected for symmetry reasons.

As a first approximation, the potential φ depends only on r and t and the velocity components (10a,b) become

$$\begin{aligned} u &= -\frac{k\rho g}{\mu}\frac{\partial h}{\partial r}, \\ w &= 0, \end{aligned} \tag{11a,b}$$

while the pressure distribution is hydrostatic and the equipotential surfaces are cylinders coaxial to the axisymmetric intruding current. These are known as Dupuit assumptions, extended to unsteady flows by Boussinesq; they constitute a good approximation in regions where the curvature of the interface is small and the flow is mainly horizontal, but can lead to paradoxes (Bear, 1988).

To develop a higher order approximation, we introduce the arbitrary length scales r^* and h^* in the horizontal and vertical directions, respectively, and the arbitrary time scale t^*. Introducing the non dimensional variables $\tilde{r} = r/r^*, \tilde{z} = z/z^*, \tilde{t} = t/t^*$, the dimensionless version of Laplace Eq. (8) reads in cylindrical coordinates under symmetry:

$$\frac{1}{\tilde{r}}\varphi_{,\tilde{r}} + \varphi_{,\tilde{r}\tilde{r}} + \frac{1}{\varpi^2}\varphi_{,\tilde{z}\tilde{z}} = 0, \ \varpi = \frac{h^*}{r^*}, \tag{12}$$

where subscripts following a comma indicate partial differentiation. Let us assume that the potential $\varphi(\tilde{z},\tilde{r},\tilde{t})$ can be expressed in a series of terms

$$\begin{aligned} \varphi &= \varphi_0(\tilde{r},\tilde{t}) + \tilde{z}\varphi_1(\tilde{r},\tilde{t}) + \tilde{z}^2\varphi_2(\tilde{r},\tilde{t}) + \ldots + \tilde{z}^n\varphi_n(\tilde{r},\tilde{t}) \\ &\equiv \sum_{n=0}^{\infty}\tilde{z}^n\varphi_n(\tilde{r},\tilde{t}). \end{aligned} \tag{13}$$

It then follows that the two terms appearing in the Laplace Eq. (12), are

$$\begin{aligned} &\frac{1}{\tilde{r}}\varphi_{,\tilde{r}} + \varphi_{,\tilde{r}\tilde{r}} = \frac{1}{\tilde{r}}\varphi_{0,\tilde{r}} + \varphi_{0,\tilde{r}\tilde{r}} + \frac{\tilde{z}}{\tilde{r}}\varphi_{1,\tilde{r}} + \tilde{z}\varphi_{1,\tilde{r}\tilde{r}} + \ldots + \frac{\tilde{z}^n}{\tilde{r}}\varphi_{n,\tilde{r}} + \tilde{z}^n\varphi_{n,\tilde{r}\tilde{r}} \\ &\equiv \sum_{n=0}^{\infty}\tilde{z}^n\left(\frac{1}{\tilde{r}}\varphi_{n,\tilde{r}} + \varphi_{n,\tilde{r}\tilde{r}}\right), \\ &\varphi_{,\tilde{z}\tilde{z}} = 2\varphi_2 + 6\tilde{z}\varphi_3 + \ldots + n(n-1)\tilde{z}^{n-2}\varphi_n \equiv \sum_{n=0}^{\infty}(n+2)(n+1)\tilde{z}^n\varphi_{n+2}. \end{aligned} \tag{14a,b}$$

Substituting (14a,b) in (12) yields

$$\sum_{n=0}^{\infty}\left[\frac{1}{\tilde{r}}\varphi_{n,\tilde{r}} + \varphi_{n,\tilde{r}\tilde{r}} + \frac{1}{\varpi^2}(n+1)(n+2)\varphi_{n+2}\right]\tilde{z}^n = 0. \tag{15}$$

Eq. (15) is satisfied for every value of the argument $\tilde{z}$ only if all the terms in square brackets are individually equal to zero, i.e.:

$$\begin{aligned} &\frac{1}{\tilde{r}}\varphi_{0,\tilde{r}} + \varphi_{0,\tilde{r}\tilde{r}} + \frac{2}{\varpi^2}\varphi_2 = 0, \\ &\frac{1}{\tilde{r}}\varphi_{1,\tilde{r}} + \varphi_{1,\tilde{r}\tilde{r}} + \frac{6}{\varpi^2}\varphi_3 = 0, \\ &\ldots \\ &\frac{1}{\tilde{r}}\varphi_{n,\tilde{r}} + \varphi_{n,\tilde{r}\tilde{r}} + \frac{1}{\varpi^2}(n+1)(n+2)\varphi_{n+2} = 0. \end{aligned} \tag{16}$$

The last expression is a recursive formula and gives the expression of the nth term as a function of the $(n-2)$th term.

The no-flow condition at the horizontal bottom (9a,b) requires that:

$$\sum_{n=0}^{\infty}(n+1)\tilde{z}^n\varphi_{n+1} = 0, \text{at } \tilde{z} = 0. \tag{17}$$

Since all the terms in the summation are zero in $\tilde{z} = 0$ except φ_1, Eq. (17) is satisfied if $\varphi_1 = 0$. As a consequence of the recursive formula, all the terms of the series with odd indices are null and the series (13) can be written as

$$\varphi = \varphi_0 - \underbrace{\frac{\varpi^2}{2}\tilde{z}^2\left(\frac{1}{\tilde{r}}\varphi_{0,\tilde{r}} + \varphi_{0,\tilde{r}\tilde{r}}\right)}_{\text{first order term}} + O(\varpi^4). \tag{18}$$

The former expression is known as the Rayleigh expansion since it was originally introduced by Rayleigh for modelling the gravity water waves propagation over a flat impermeable bed. Eq. (18) approximates an infinite series, and the magnitude of the first omitted term corresponds to the magnitude of all omitted terms providing that the expansion is asymptotic in the domain for $\varpi \to 0$. In (18), φ_0, is defined as the zeroth order term, while the first order term has coefficient ϖ^2, and so on.

Reverting to dimensional form, it is immediate to obtain the velocity field upon deriving Eq. (18) as

$$\mathbf{u} = \underbrace{-\frac{k}{\mu}\rho g \nabla\varphi_0}_{\text{zeroth order term}} + \underbrace{\frac{k\rho g}{2\mu}\nabla\left(z^2\left(\frac{1}{r}\varphi_{0,r} + \varphi_{0,rr}\right)\right)}_{\text{first order term}} + \ldots, \tag{19}$$

where terms of order $O(\varpi^4)$ were neglected. The velocity components become in cylindrical coordinates

$$u = \underbrace{-\frac{k}{\mu}\rho g\varphi_{0,r}}_{\text{zeroth order term}} + \underbrace{\frac{k\rho g}{2\mu}\left(\frac{1}{r}\varphi_{0,rr} - \frac{1}{r^2}\varphi_{0,r} + \varphi_{0,rrr}\right)z^2}_{\text{first order term}} + \ldots,$$
$$w = \underbrace{\frac{k\rho g}{\mu}\left(\frac{1}{r}\varphi_{0,r} + \varphi_{0,rr}\right)z}_{\text{first order term}} + \ldots. \tag{20a, b}$$

The equivalent of the series in Eq. (20a,b) was introduced in Nielsen et al. (1997) for planar free surface seepage flow over a horizontal bed, with the adoption of an infinite order operator. The vertical velocity (20a,b) shows a linear variation with z, as in Yortsos (1995), Nielsen et al. (1997) and Knight (2005).

At the zeroth order, Eqs. (9a,b-18) indicate that at the interface

$$\varphi_0 = \frac{\Delta\rho}{\rho}h, \tag{21}$$

and assuming that (21) approximately holds at higher orders, Eq. (20a,b) recasts as

$$u = \underbrace{-\frac{k\Delta\rho g}{\mu}\frac{\partial h}{\partial r}}_{\text{zeroth order term}} + \underbrace{\frac{k\Delta\rho g}{2\mu}\left(\frac{1}{r}\frac{\partial^2 h}{\partial r^2} - \frac{1}{r^2}\frac{\partial h}{\partial r} + \frac{\partial^3 h}{\partial r^3}\right)z^2}_{\text{first order term}} + \ldots,$$
$$w = \underbrace{\frac{k\Delta\rho g}{\mu}\left(\frac{1}{r}\frac{\partial h}{\partial r} + \frac{\partial^2 h}{\partial r^2}\right)z}_{\text{first order term}} \ldots. \tag{22a, b}$$

Note that (i) the approximation at the interface, with $\varphi \approx \varphi_0 = (\Delta\rho/\rho)h$ is a linearisation of the differential problem, since we include higher terms in the expression of the potential but impose the boundary condition at the interface corresponding to the zeroth order field. As a consequence, the pressure field is independent on the interface as modulated by higher order terms of the potential and is computed referring to the zeroth order. In this respect, similar approximations have been used and discussed by several authors (see, e.g., Dagan, 1967; Dagan and Bear, 1968; Nordbotten and Celia, 2006); (ii) truncating the terms of order ϖ^4 is consistent with the assumption that the potential is expressed by an asymptotic expansion.

Introducing Eq. (22a,b) in Eq. (7) and integrating results in

$$\frac{k}{\mu}\Delta\rho g\frac{1}{r}\frac{\partial}{\partial r}\left(rh\frac{\partial h}{\partial r} - r\frac{h^3}{6}\left(\frac{1}{r}\frac{\partial^2 h}{\partial r^2} - \frac{1}{r^2}\frac{\partial h}{\partial r} + \frac{\partial^3 h}{\partial r^3}\right)\right) = \phi\frac{\partial h}{\partial t}. \tag{23}$$

Moreover, global continuity requires

$$2\pi\phi\int_0^{r_N(t)} rh(r,t)dr = Qt^{\alpha}. \tag{24}$$

Introducing the dimensionless variables $T = t/t^*, R = r/r^*, R_N = r_N/r^*, H = h/r^*, Z = z/r^*, U = u/v^*, W = w/v^*$ where the time, space and velocity scales are $t^* = \left[Q/(\phi v^{*3})\right]^{1/(3-\alpha)}$, $r^* = v^* \cdot t^*$, $v^* = \Delta\rho g k/(\phi\mu)$, recasts Eqs. (23) and (24) for $\alpha \neq 3$ as

$$\frac{1}{R}\frac{\partial}{\partial R}\left[RH\frac{\partial H}{\partial R} - \frac{1}{6}H^3\frac{\partial^2 H}{\partial R^2} + \frac{1}{6}\frac{H^3}{R}\frac{\partial H}{\partial R} - \frac{1}{6}RH^3\frac{\partial^3 H}{\partial R^3}\right] - \frac{\partial H}{\partial T} = 0, \tag{25}$$

$$2\pi\int_0^{R_N(T)} RHdR = T^{\alpha}, \tag{26}$$

and Eq. (4) as

$$H(R_N(T), T) = 0. \tag{27}$$

The dimensionless velocities become

$$U = -\phi\left[\frac{\partial H}{\partial R} + \left(\frac{1}{R^2}\frac{\partial H}{\partial R} - \frac{1}{R}\frac{\partial^2 H}{\partial R^2} - \frac{\partial^3 H}{\partial R^3}\right)\frac{Z^2}{2}\right],$$
$$W = \phi\left(\frac{1}{R}\frac{\partial H}{\partial R} + \frac{\partial^2 H}{\partial R^2}\right)Z. \tag{28a, b}$$

For $\alpha = 3$ the time scale defined above is no longer valid and a new velocity scale enters the problem, $v_1^* = (Q/\phi)^{1/3}$ (Vella and Huppert, 2006). With the new set of dimensionless variables $T = t/t^*, R = r/r^*, R_N = r_N/r^*, H = h/r^*, Z = z/r^*, U = u/v^*, W = w/v^*$ where the space scale is $r^* = (Q/\phi)^{1/3} \cdot t^*$, and the time scale t^* is arbitrary, Eqs. (23) and (24) give

$$\frac{\delta_r}{R}\frac{\partial}{\partial R}\left[RH\frac{\partial H}{\partial R} - \frac{1}{6}H^3\frac{\partial^2 H}{\partial R^2} + \frac{1}{6}\frac{H^3}{R}\frac{\partial H}{\partial R} - \frac{1}{6}RH^3\frac{\partial^3 H}{\partial R^3}\right] - \frac{\partial H}{\partial T} = 0, \tag{29}$$

$$2\pi\int_0^{R_N(T)} RHdR = T^3, \tag{30}$$

where $\delta_r = v^*/v_1^*$ is the ratio between the two velocity scales, while the boundary condition expressed by Eq. (26) still holds.

3. Solution of the problem

The differential problem given by (24)–(26) requires a numerical solution for the general case $\alpha \neq 3$, while it admits a similarity solution for the special case $\alpha = 3$ (Eqs. (24)–(26) reduce to (28)–(29) together with (26)). It is worth noting that in the context of a different study on viscous gravity currents, namely 2-D free-surface intrusions flowing over a deep porous medium, Acton et al. (2001) similarly found that self-similar solutions could be obtained only for $\alpha = 3$.

3.1. Self-similar solution

Introducing the similarity variable

$$\eta = RT^{-1} \tag{31}$$

and denoting by η_N the value of η for $R = R_N(T)$, the current extension is given by

$$R_N(T) = \eta_N T. \tag{32}$$

With Eq. (31), the similarity solutions of Eqs. (28) and (29) is

$$H(R,T) = \eta_N^2 T\psi(\zeta), \zeta = \eta/\eta_N \tag{33}$$

and the differential problem given by Eqs. (28) and (29) plus Eq. (26) becomes

$$\delta_r \frac{d}{d\zeta}\left[\zeta\psi\frac{d\psi}{d\zeta} + \underbrace{\frac{1}{6}\psi^3\left(\frac{1}{\zeta}\frac{d\psi}{d\zeta} - \frac{d^2\psi}{d\zeta^2} - \zeta\frac{d^3\psi}{d\zeta^3}\right)}_{\text{first order correction}}\right] + \zeta^2\frac{d\psi}{d\zeta} - \zeta\psi = 0,$$

$$\eta_N = \left(2\pi\int_0^1 \zeta\psi(\zeta)d\zeta\right)^{-1/4},$$

$$\psi(\zeta = 1) = 0. \tag{34a, b, c}$$

The dimensionless velocities are, for $Z \leqslant H(R,T)$,

$$U = -\phi\eta_N\left[\frac{d\psi}{d\zeta} + \left(\frac{d\psi}{d\zeta} - \zeta\frac{d^2\psi}{\partial\zeta^2} - \zeta^2\frac{d^3\psi}{\partial\zeta^3}\right)\frac{Z^2}{2R^2}\right],$$

$$W = \phi\eta_N\left(\frac{d\psi}{d\zeta} + \zeta\frac{d^2\psi}{\partial\zeta^2}\right)\frac{Z}{R}. \tag{35a,b}$$

The numerical integration of the fourth order differential equation in (34a,b,c) requires specifying four boundary conditions at $\zeta = 1 - \varepsilon$, with ε being a small quantity. To obtain these, we develop a Frobenius expansion of (34a,b,c) near the current tip. Introducing the variable $\chi = 1 - \zeta$, we seek a solution as $\chi \to 0$ in the form:

$$\psi(\chi) = \sum_0^\infty a_k\chi^{k+b}, \tag{36}$$

where b is the indicial exponent. Eq. (36) already fulfils the boundary condition $\psi(\chi \to 0) = 0$. Equating the exponents of the lowest powers of χ (for $k = 0$) gives $b = 1$, while equating to zero the coefficients of powers of χ yields:

$$a_0 = \frac{1}{\delta_r}, a_1 = \frac{1}{4\delta_r}, a_2 = \frac{2 - 3\delta_r^2}{8\delta_r - 24\delta_r^3}. \tag{37a, b, c}$$

Upon considering the first three terms of the Frobenius series, the four boundary conditions at $\chi = \varepsilon$ are obtained as

$$\psi|_{\zeta=1-\varepsilon} = a_0\varepsilon + a_1\varepsilon^2 + a_2\varepsilon^3,$$

$$\left.\frac{\partial\psi}{\partial\zeta}\right|_{\zeta=1-\varepsilon} = -a_0 - 2a_1\varepsilon - 3a_2\varepsilon^2,$$

$$\left.\frac{\partial^2\psi}{\partial\zeta^2}\right|_{\zeta=1-\varepsilon} = 2a_1 + 6a_2\varepsilon, \tag{38a, b, c, d}$$

$$\left.\frac{\partial^3\psi}{\partial\zeta^3}\right|_{\zeta=1-\varepsilon} = -6a_2.$$

Fig. 2 shows the comparison between the shape factor ψ obtained by numerically integrating (34a,b,c) with (38a,b,c,d) and the zeroth order approximation solution by Lyle et al. (2005) for

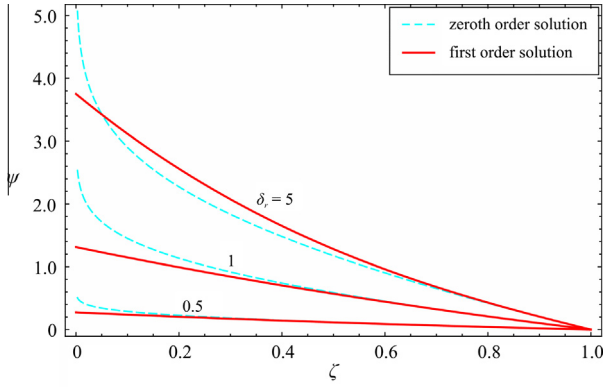

Fig. 2. Shape factor ψ as a function of the scaled similarity variable ζ for $\alpha = 3$ and $\delta_r = 0.5, 1, 5$.

$\alpha = 3$ and three different values of δ_r. For $\delta_r < 1$ the first-order solution yields lower values of the shape factor than the zeroth order solution, and does not exhibit an asymptote in the origin. Once the shape function ψ and prefactor η_N are known, dimensionless and dimensional expressions of the current extension and profile are derived via (32) and (33).

3.2. Numerical solution

For $\alpha \neq 3$, numerical integration of (24)–(26) is required. To overcome the problems due to the changing boundary R_N, the domain $[0, R_N]$ is mapped onto $[0,1]$ by introducing the transformation $H(R, T) \to H(y(R, T), T)$, with $y = R/R_N(T)$, resulting in the following equations

$$\frac{\partial H}{\partial T} = \frac{\dot{R}_N}{R_N}y\frac{\partial H}{\partial y} + \frac{1}{R_N^2}\frac{1}{y}\frac{\partial}{\partial y}\left[yH\frac{\partial H}{\partial y} - \frac{1}{6R_N^2}H^3\frac{\partial^2 H}{\partial y^2} + \frac{1}{6R_N^2}\frac{H^3}{y}\frac{\partial H}{\partial y} - \frac{1}{6R_N^2}yH^3\frac{\partial^3 H}{\partial y^3}\right], \tag{39}$$

$$2\pi R_N^2\int_0^1 yHdy = T^\alpha, \tag{40}$$

where the dot indicates the time derivative, while the boundary condition given by (26) becomes

$$H(1, T) = 0. \tag{41}$$

A second-order, centred differences scheme was used for the spatial derivatives and a Crank-Nicolson implicit algorithm for the time derivatives. Some of the coefficients in Eq. (39) are singular at $y = 1$; in this case the asymptotic expression

$$H \sim R_N\dot{R}_N(1 - y) + \frac{R_N\dot{R}_N\left(\dot{R}_N^2 - 2\right)}{6\left(\dot{R}_N^2 - 3\right)}(1 - y)^3 \tag{42}$$

was used. The non-linear system of equations to be solved at each time step was approached through a Levenberg–Marquardt algorithm, imposing the flux near the origin as

$$\lim_{y\to 0}\left[2\pi yH\frac{\partial H}{\partial y}\right] = -\alpha T^{\alpha-1}. \tag{43}$$

The speed of the current front was calculated via the difference of the positions of the leading edge at two subsequent time steps. The accuracy and consistency of the algorithm was tested comparing the numerical results with the theoretical self-similar solution for $\alpha = 3$. The scheme was found to converge to four significant figures employing 100 grid points and time steps initially equal to 10^{-3}; the numerical solution was independent of further refinement of grid spacing and time-step size. Noteworthy, for increasing R_N the terms of the first order correction become negligible with respect to the other terms, and the zeroth order solution is sufficient to describe the flow correctly.

The dimensionless horizontal and vertical velocities given by (27a,b) are plotted in Fig. 3 for $\alpha = 1$, two values of dimensionless time $T = 0.5$, 1.0 and several values of the rescaled similarity variable ζ. It is seen that both velocities decrease with increasing values of time and similarity variable; the vertical velocity is a small fraction of the horizontal velocity except for $\zeta < 0.4$ and at early times. At the front end the vertical component is null and the horizontal velocity equals the front end velocity.

4. Experimental observations and uncertainty analysis

The theoretical model was tested against laboratory experiments in which a constant ($\alpha = 1.0$) or time increasing flux ($\alpha = 1.5$) of pure glycerol, or of a mixture of glycerol and water,

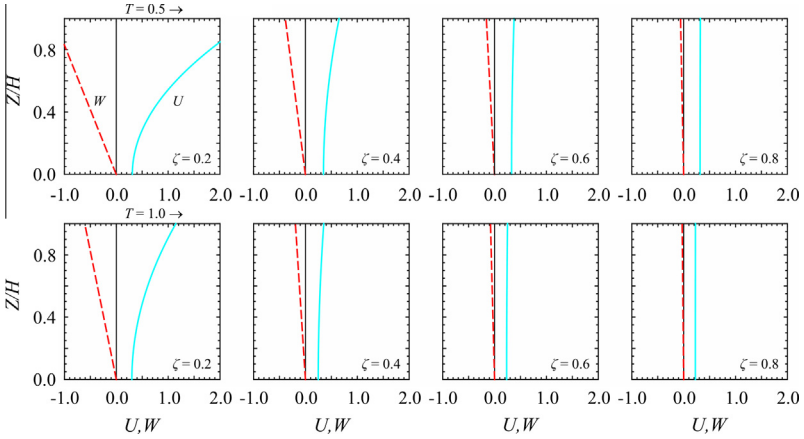

Fig. 3. Dimensionless horizontal and vertical velocities U, W profiles for $\alpha = 1$ and different values of similarity variable ζ; upper panels: time $T = 0.5$; lower panels: time $T = 1.0$.

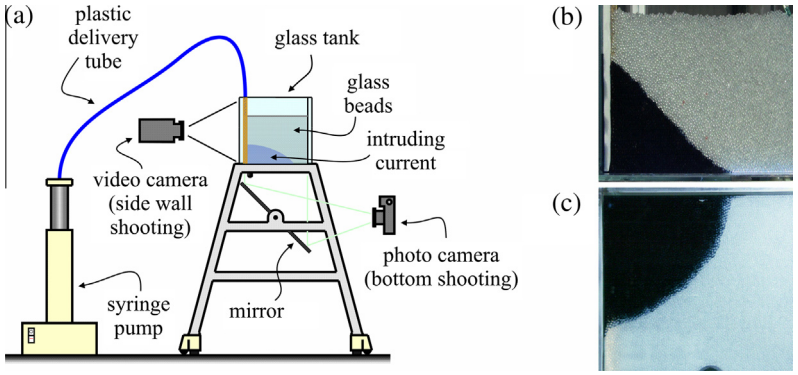

Fig. 4. (a) Sketch of the experimental apparatus, including the tank, the pump and the cameras to acquire the lateral and the bottom profile of the intruding current. (b) A snapshot and (c) a plane bottom view of the intruding current for test #16.

was released in a porous medium made of uniform glass beads and initially saturated with air. The experiments were described in detail in Longo et al. (2013) and are briefly summarised here.

The experimental apparatus and the devices employed are shown in Fig. 4. The experiments were performed in a square glass tank $25 \times 25 \times 25\ \mathrm{cm}^3$ filled with glass beads with diameter $d = 3$ mm. The intruding fluid was injected with a syringe pump Teledyne ISCO 260D, with an accuracy of 0.5%, controllable with an analogue electric signal in order to vary the flow rate, if requested. The fluid was injected through a 1-mm internal diameter tube inserted in a cylindrically shaped injection volume, or 'well', located in a corner of the tank and having permeable walls constructed with brass net. The lateral profile of the current was recorded by a video camera (1920×1080 pixels) at 25 frames per second; a photo camera (3456×2304 pixels) was used to record the radial spreading of the current from the bottom. Several algorithms were used to process the images in order to obtain a planar, undistorted and calibrated image and to detect the boundary between the intruding current (darkened through a modest addition of ink) and the ambient fluid (air). The overall uncertainty in detecting the boundary is equal to ±1 mm. The data representing the front end position and the profile of the intruding current were averaged in space (over 10 glass beads diameters) and then under sampled with a step of one bead diameter. The permeability of the porous medium was evaluated from the porosity ϕ of the medium and the diameter d of the glass beads using the Kozeny-Carman equation $k = \phi^3 d^2/[180(1-\phi)^2]$.

In order to assess the accuracy of the theoretical model in reproducing the experimental results, it is necessary to include in the computations the effect of the uncertainties in the parameters. In the Appendix, we describe how the sensitivity of the model to parameter uncertainties is evaluated, and provide a synthetic example assuming a fictitious coefficient of variation equal to 1% for each variable. Here, we discuss the actual values of the uncertainties affecting the key problem parameters, i.e. μ, $\Delta\rho$, ϕ, d and Q_d, in the present set of experiments.

The numerical value of the dynamic viscosity is affected by the uncertainties in the rheometer and in the linear regression of the experimental data of measured shear stress and shear rate; as a consequence, the standard deviation of μ can be assumed for our test to be equal to 3.5% of the average value. Uncertainties in measurements of density difference $\Delta\rho$ and total flow rate Q_d are specific to devices adopted in our experiments and, on the base of their characteristics and of the manufacturer's specifications, a relative error of ±1% for $\Delta\rho$, and ±0.5% for Q_d is considered. The manufacturer's specifications for the glass beads indicate a tolerance of 5% on the nominal diameter, which is assumed as the value of the standard deviation of d. Not many indications can be extracted from literature on the variability of porosity ϕ for packs of homogeneous glass beads. Aste et al. (2004) indicate experimental values of porosity for uniform glass beads with $d = 1.0 \pm 0.05$ mm and $d = 1.59 \pm 0.05$ mm in the range 0.36–0.41 with a normal distribution and a standard deviation of 1.5%. The experimental distribution of the porosity shown by Bloom et al., 2009 allows

Table 1
Parameter values for three tests from Longo et al. (2013). The uncertainty is expressed as one standard deviation.

Test #	Q_d (ml/s)	α	$\Delta\rho$ (kg m^{-3})	μ (Pa s)	d (mm)	ϕ
16	4.0 ± 0.5%	1.0	1250 ± 1%	0.58 ± 3.5%	3.0 ± 5%	0.38 ± 1%
17	4.0 ± 0.5%	1.0	1145 ± 1%	0.012 ± 3.5%	3.0 ± 5%	0.38 ± 1%
18	0.06 $t^{1/2}$ ± 0.5%	1.5	1241 ± 1%	0.26 ± 3.5%	3.0 ± 5%	0.38 ± 1%

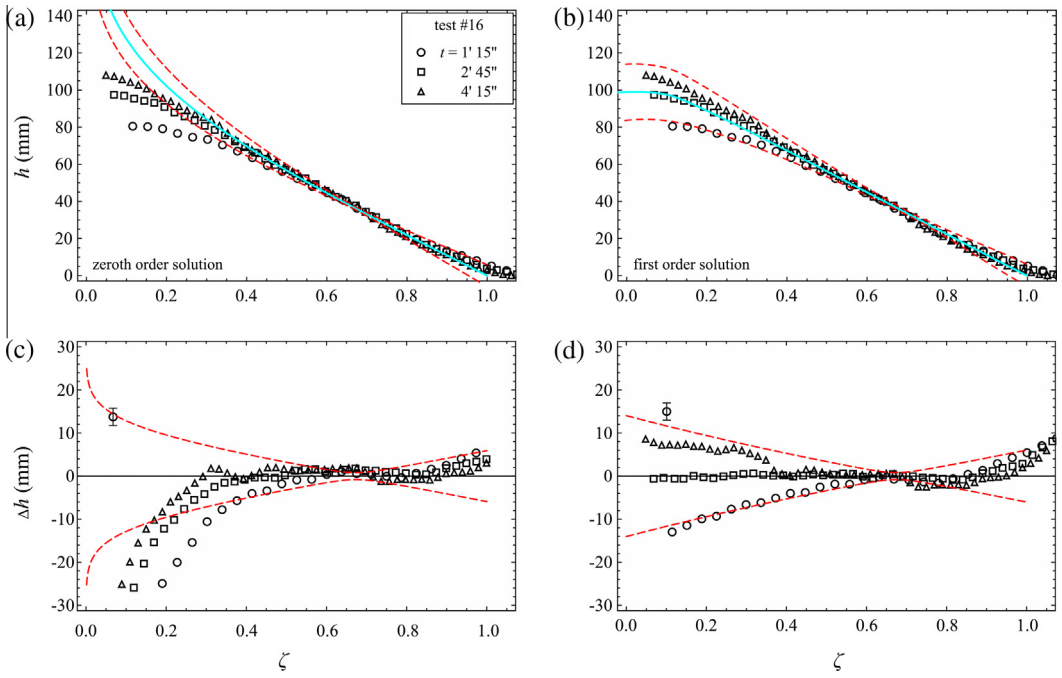

Fig. 5. The height of the gravity current as a function of radial coordinate, (a) zero order solution, (b) first order solution. (c) Residuals for the zero order solution and (d) for the first order solution. The dashed lines are the 95% confidence limits, the error bar indicates the uncertainty at 95% level of confidence. Results for test #16, μ = 0.58 ± 3.5% Pa s, $\Delta\rho$ = 1250 ± 1% kg/m^3, Q_d = 4.0 ± 0.5% ml/s, α = 1.0, d = 3.0 ± 5% mm, ϕ = 0.38 ± 1%. The values of the parameters indicate the estimate of the average ± one standard deviation.

to infer a standard deviation of less than 1%. Hence in the present analysis we assume a standard deviation of porosity equal to 1%.

Table 1 lists the input values for the three tests of interest in Longo et al. (2013), and the associated uncertainty.

Panels (a) and (b) of Fig. 5 show the comparison between the two models (the zeroth and the first order) and the experimental profile in test #16 at different times. The theoretical profile is determined by assuming the nominal mean values of the parameters. The improvement of the first order correction over the zeroth order solution in interpreting experimental results is appreciable approximately up to one third of the current length, and is evident near the origin, where the refined solution does not result in an asymptotic profile as the zeroth order one.

Panels (c) and (d) of the same Figure show the residuals of the experimental data for test #16 and the 95% confidence limits for the zeroth order solution and for the first order solution, assuming that the uncertainties are those reported in Table 1. The residuals with respect to the zeroth order solution are included in the confidence band except near the origin, whereas the residuals with respect to the first order solution lie practically always within the confidence limits.

Fig. 6 shows the contribution to the coefficient of variation (CV) of the current height for test#16 in Longo et al. (2013) due to the five uncertain parameters. The dominant contribution is due to the diameter d, with a significant contribution coming also from the porosity ϕ; the other parameters are less important. The overall profile of the total CV is qualitatively similar to that derived for

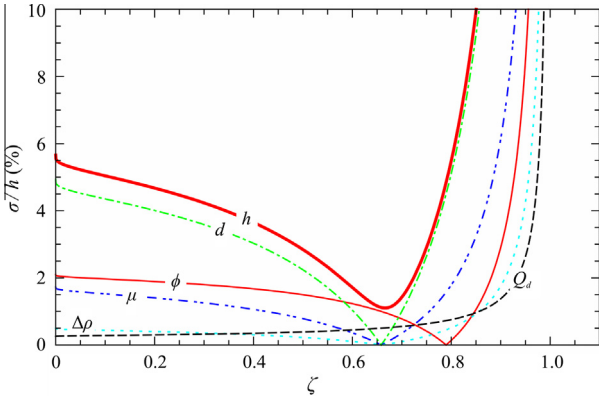

Fig. 6. Contributions to the coefficient of variation (CV) of the height of the current. Results for test #16, μ = 0.58 ± 3.5% Pa s, $\Delta\rho$ = 1250 ± 1% kg/m^3, Q_d = 4.0 ± 0.5% ml/s, α = 1.0, d = 3.0 ± 5% mm, ϕ = 0.38 ± 1%.

the illustrative example shown in Fig. A1 in the Appendix, with fictitious standard deviations as opposed to real ones, in that at two-thirds of the total current length the relative uncertainty reaches a minimum and then increases asymptotically near the front end. A more extended comparison with the experimental results for tests #17 and #18 is shown in the Supplementary Material, available online. Results of the comparison for the profile

Table 2
Parameter values for the experiments described in Lyle et al. (2005). The reduced gravity listed in the original paper has been converted by assuming that the mass density of the ambient fluid is $\rho = 1000$ kg m^{-3}. The uncertainty is considered equal to a single standard deviation. Data on the uncertainties of the parameters are not reported in the original paper and have been kindly communicated by Hallworth (2013) (personal communication).

Expt	1	2	3	4	5	6
$\Delta\rho$ (kg m^{-3})	10.2 ± 0.3	20.4 ± 0.3	40.8 ± 0.3	81.6 ± 0.3	40.8 ± 0.3	40.8 ± 0.3
Q_d (ml s^{-1})	36.8 ± 0.2	34.4 ± 0.2	34.4 ± 0.2	39.2 ± 0.2	9.2 ± 0.2	72.4 ± 0.2

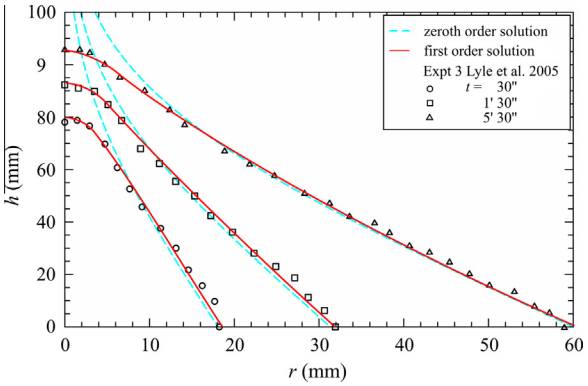

Fig. 7. The height of the gravity current as a function of radial coordinate. Dashed line: zeroth order solution. Bold line: first order solution. Symbols: experiment 3 from Lyle et al., 2005, $\mu = 1.2 \times 10^{-3}$ Pa s, $\Delta\rho = 40$ kg/m^3, $Q_d = 34.4$ ml/s, $\alpha = 1.0$, $\phi = 0.37$, $k = 6.8 \times 10^{-9}$ m^2.

are qualitatively similar, except that the fitting is better and confidence intervals are narrower for test #17.

Finally, a comparison between the theoretical solution and experimental results was carried out also in terms of the radius of the current, as described in detail in the Appendix. When compared to the zeroth order result, the first order solution yields a slightly larger spreading rate at early times, converging to the zeroth order solution at late times. It is seen that adoption of either solution is immaterial in interpreting experimental results in terms of the radius of propagation.

5. Comparison of theoretical model with experimental results by Lyle et al. (2005)

Lyle et al. (2005) performed nine experiments with radial gravity currents of Newtonian fluid by using an apparatus similar to that employed in our experiments (Longo et al., 2013). Six of the experiments are of interest for the present analysis; the parameter values for these tests are listed in Table 2. In their experiments, the reduced gravity is very low since the intruding fluid (salt water mixtures with different absolute salinity) was injected in a porous medium filled with fresh water. The porous medium consisted of 3.0 mm diameter glass ballotini, with a tolerance communicated by the manufacturer equal to −0.15, +0.30 mm. The viscosity of the intruding fluid is estimated from literature data (Sharqawy et al., 2010), and is assumed equal to $\mu = 1.2 \cdot 10^{-3} \pm 1\%$ Pa s for all salt water mixtures at $\Theta = 20$ °C (the absolute salinity of the mixture has a minor effect on the viscosity). The porosity is taken to be $\phi = 0.37 \pm 1\%$.

Fig. 7 shows the current profile as a function of the distance from the origin at three different times for Expt 3. The dashed line is the zeroth order solution, the bold line the first order solution. The data collapse on the zeroth order solution is satisfactory far from the origin and fails near the origin, due to the boundary effect of the injection well. On the contrary, the first order solution agrees with the experiments in the whole spatial range.

Additional comparisons are included in the Supplementary Material available online, describing results for the remaining experiments by Lyle et al. (2005). These demonstrate again the narrowing of confidence limits associated with the first order correction.

6. Conclusions

Our work leads to the following major conclusions:

- An improved solution for spreading of axisymmetric gravity currents in uniform porous media was derived adopting a Rayleigh expansion of the Darcy velocity potential at first order. The new formulation allows for nonzero vertical velocities, effectively removing the Dupuit–Forchheimer assumption, and eliminates the asymptote of the shape factor present in the origin at zeroth order. The solution is self-similar for $\alpha = 3$.
- An extensive comparison of the zeroth and first order theoretical models with two sets of experiments was carried out, together with a statistical analysis of the uncertainties affecting model results and experimental data.
- Profiles obtained with the first order solution have a finite height in the origin and depend almost linearly on the distance from the origin, as experimentally detected by Lyle et al. (2005). The refined model exhibits a much better agreement with experimental data than the zeroth order model near the origin, where the free surface curvature is relevant and the vertical velocity of the interstitial fluid is non-negligible. Only experimental profiles at early times, still reminiscent for a large part of their extension of the boundary effects induced by the injection, do not match the theoretical model. The prediction of the profile is consistently accurate and with a narrow band of confidence.
- The effect of the correction is much less important for the radius of propagation, which in the first order solution always increases, albeit modestly, with respect to the zeroth order solution. This is due to the lesser volume stored in the porous medium near the origin, which in turn is compensated by a larger volume stored near the front, in order to balance the injected mass. However, due to the radial geometry of the system, a limited increase in the radius of propagation is sufficient to induce a relevant increment in the stored volume of liquid. Experimental results for the current radius of propagation compare well with either model, since the differences between models are of the same order of the associated uncertainties.
- In our experiments the contribution to the coefficient of variation (CV) of the current profile due to uncertainty in model parameters is largest for the diameter d, with a significant contribution coming also from the porosity ϕ; the other parameters are less important. In general the sensitivity analysis indicates that porosity (directly affecting, with the diameter d, the intrinsic permeability) is the main source of uncertainty hence, in controlled experiments, a great deal of attention should be paid in reproducing the porous medium with uniform known porosity.

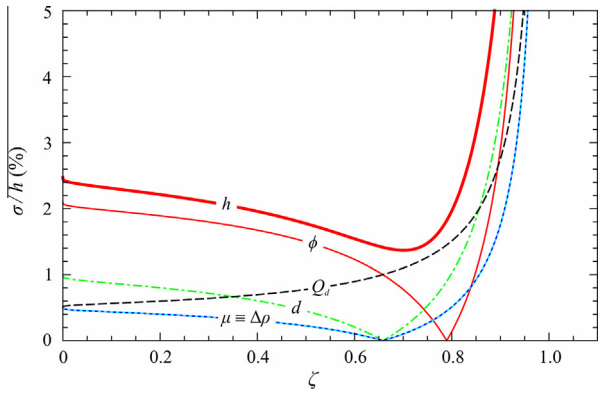

Fig. A1. Contributions to the coefficient of variation (CV) of the height of the current. It is assumed that the CV of the parameters is 1%. Results for test #16, $\mu = 0.58 \pm 1\%$ Pa s, $\Delta\rho = 1250 \pm 1\%$ kg/m^3, $Q_d = 4.0 \pm 1\%$ ml/s, $\alpha = 1.0$, $d = 3.0 \pm 1\%$ mm, $\phi = 0.38 \pm 1\%$.

Acknowledgements

Data on the uncertainties of the parameters in the experiments reported in Lyle et al. (2005) were not reported in the original paper and have been kindly communicated by Mark Hallworth. We also acknowledge the revisions of the anonymous Reviewers that greatly improved the readability and the clarity of the manuscript.

Appendix A

A.1. Model sensitivity analysis

This Appendix illustrates the general procedure used to conduct the model sensitivity analysis to uncertainties in the parameters. The output of the model (based on the zero order solution) is represented by the profile of the intruding current, a generic function f of time, radial coordinate and five additional parameters:

$$h = f(r, t, \phi, d, Q_d, \Delta\rho, \mu), \tag{25}$$

assuming that gravity is fixed and invariable, the flow rate is constant, and α is exempt from uncertainty. Considering the parameters to be independent random variables and adopting the usual rules for error propagation (developing in Taylor series and neglecting the second derivatives, e.g. Navidi, 2006), the standard deviation of h is

$$\sigma_h = F(r, t, \bar{\phi}, \bar{d}, \overline{Q_d}, \overline{\Delta\rho}, \bar{\mu}, \sigma_\phi, \sigma_d, \sigma_{Q_d}, \sigma_{\Delta\rho}, \sigma_\mu), \tag{25}$$

where F is another generic function, the over bar denotes the mean value and σ stands for standard deviation. Note that we do not need to assume a specific probability distribution of the random parameters and only the estimates of their mean value and standard deviation are required. To have an accurate estimation by considering only the first term of the Taylor series, it is also necessary that the standard deviation values are small with respect to the mean values of the variables.

In order to illustrate the typical output of an uncertainty analysis, Fig. A1 shows the contribution to the total standard deviation of the height of the intruding current due to the uncertainty of the fluid viscosity, the discharge, the diameter of glass beads, the density and the porosity in test #16, assuming the coefficient of variation to be equal to 1% for each variable. The higher contribution is due to the porosity, which is dominant at least till a distance equal to 50% of the front end position. The second most important contribution comes from the discharge. At approximately $\zeta = 0.7$ the relative variance of the profile height has a minimum, after which it grows asymptotically near the front end. The fluid viscosity and the density give an identical, and lowest, contribution.

Appendix B. Supplementary material

Supplementary associated with this article can be found, in the online version, at http://dx.doi.org/10.1016/j.jhydrol.2014.07.003.

References

Acton, J.M., Huppert, H.E., Worster, M.G., 2001. Two-dimensional viscous gravity currents flowing over a deep porous medium. J. Fluid Mech. 440, 359–380.
Aste, T., Saadatfar, M., Sakellariou, A., Senden, T.J., 2004. Investigating the geometrical structure of disordered sphere packings. Physica A – Stati. Mech. Appl. 339 (1–2), 16–23.
Barenblatt, G.I., Zel'dovich, Y., 1957. On dipole solutions in problems of non-stationary filtration of gas under polytropic regime. Prikl. Math. Mekh. 21 (5), 718–720.
Bear, J., 1988. Dynamics of Fluids in Porous Media. Dover.
Bickle, M., Chadwick, A., Huppert, H.E., Hallworth, M., Lyle, S., 2007. Modelling carbon dioxide accumulation at Sleipner: implications for underground carbon storage. Earth Planet. Sci. Lett. 255 (1-2), 164–176.
Bloom, M., Russel, M., Kustau, A., Muriel, K., Mandayam, S., Sukumaran, B., 2009. Measurement of Granular Material Packing. in: AIP Conf. Proc., 1145, 195–198.
Dagan, G., 1967. Second-order theory of shallow free-surface flow in porous media. Quart. J. Mech Appl. Math. XX (4), 517–526.
Dagan, G., 1968. A derivation of Dupuit solution of steady flow toward wells by matched asymptotic expansions. Water Resour. Res. 4 (2), 403–412.
Dagan, G., Bear, J., 1968. Solving the problem of local interface upconing in a coastal aquifer by the method of small perturbations. J. Hydraul. Res. 6 (1), 15–44.
de Loubens, R., Ramakrishnan, T.S., 2011. Analysis and computation of gravity-induced migration in porous media. J. Fluid Mech. 675, 60–86.
Di Federico, V., Archetti, R., Longo, S., 2012. Spreading of axisymmetric non-Newtonian power-law gravity currents in porous media. J. Non-Newton. Fluid Mech. 189–190, 31–39.
Di Federico, V., Longo, S., Archetti, R., Chiapponi, L., Ciriello, V., 2014. Radial gravity currents in vertically graded porous media: theory and experiments for Newtonian and power-law fluids. Adv. Water Resour. 70, 65–76.
Dullien, F.A.L., 1992. Porous Media – Fluid Transport and Pore Structure. Academic Press.
Dussan, E.B., Auzerais, F.M., 1993. Buoyancy induced flow in porous media generated near a drilled oil well. Part 1. The accumulation of filtrate at a horizontal impermeable boundary. J. Fluid Mech. 254, 283–381.
Golding, M., Huppert, H.E., Neufeld, J., 2013. The effects of capillary forces on the axisymmetric propagation of two phase, constant-flux gravity currents in porous media. Phys. Fluids 25, 036602.
Golding, M., Huppert, H.E., 2010. The effect of confining impermeable boundaries on gravity currents in a porous medium. J. Fluid Mech. 649, 1–17.
Hallworth, M., 2013. Personal Commun..
Huppert, H.E., Woods, A.W., 1995. Gravity-driven flows in porous layers. J. Fluid Mech. 292, 55–69.
King, S.E., Woods, A.W., 2003. Dipole solutions for viscous gravity currents: theory and experiments. J. Fluid Mech. 483, 91–109.
Knight, J.H., 2005. Improving the Dupuit–Forchheimer groundwater free surface approximation. Adv. Water Resour. 28, 1048–1056.
Koussis, D., Mazi, K., Destouni, G., 2012. Analytical single-potential, sharp-interface solutions for regional seawater intrusion in sloping unconfined coastal aquifers, with pumping and recharge. J. Hydrol. 416–417, 1–11.
Li, L., Lockington, D.A., Parlange, M.B., Stagnitti, F., Jeng, D.S., Selker, J.S., Telyakovskiy, A.S., Barry, D.A., Parlange, J.Y., 2005. Similarity solution of axisymmetric flow in porous media. Adv. Wat. Res. 28, 1076–1082.
Longo, S., Di Federico, V., Chiapponi, L., Archetti, R., 2013. Experimental verification of power-law non-Newtonian axisymmetric porous gravity currents. J. Fluid Mech/Rapids 731, R2.
Lyle, S., Huppert, H.E., Hallworth, M., Bickle, M., Chadwick, A., 2005. Axisymmetric gravity currents in a porous medium. J. Fluid Mech. 543, 293–302.
Mathunjwa, J.S., Hogg, A.J., 2007. Freely draining gravity currents in porous media: dipole self-similar solutions with and without capillary retention. Eur. J. Appl. Math. 18, 337–362.
Navidi, W., 2006. Statistics for Engineers and Scientists. McGraw-Hill.
Nielsen, P., Aseervatham, R., Fenton, J.D., Perrochet, P., 1997. Groundwater waves in acquifers of intermediate depths. Adv. Water Resour. 20, 37–43.
Nordbotten, J.M., Celia, M.A., 2006. An improved analytical solution for interface upconing around a well. Water Resour. Res. 42, W08433.
Parlange, J.Y., Stagnitti, F., Starr, J.L., Braddock, R.D., 1984. Free surface flow in porous media and periodic solution of the shallow flow approximation. J. Hydrol. 70, 251–263.
Phillips, O.M., 1991. Flow and Reactions in Permeable Rocks. Cambridge University Press.
Pritchard, D., Woods, A.W., Hogg, A.J., 2001. On the slow draining of a gravity current moving through a layered permeable medium. J. Fluid Mech. 444, 23–47.

Sharqawy, M.H., Lienhard, J.H.V., Zubair, S.M., 2010. The thermophysical properties of seawater: a review of existing correlations and data. Desalination Water Treat. 16, 354–380.
Ungarish, M., 2010. An introduction to gravity currents and intrusions. CRC Press, Boca Raton.
Vella, D., Huppert, H.E., 2006. Gravity currents in a porous medium at an inclined plane. J. Fluid Mech. 555, 353–362.
Woods, A.W., Mason, R., 2000. The dynamics of two-layer gravity-driven flows in permeable rock. J. Fluid Mech. 421, 83–114.
Yortsos, Y.C., 1995. A theoretical analysis of vertical flow equilibrium. Transp. Porous Media 18 (2), 107–129.